On the high density in the HFS far SOL at ASDEX Upgrade and its impact on plasma confinement

S. Potzel[1], M. Dunne[1], R. Dux[1], L. Guimarais[2], F. Reimold[3], A. Scarabosio[1], M. Wischmeier[1]
the ASDEX Upgrade team and the EUROfusion MST1 Team*

[1]*Max-Planck-Institut für Plasmaphysik, Garching, Germany*
[2]*Instituto de Plasmas e Fusao Nuclear, Universidade de Lisboa, Lisboa, Portugal*
[3] *Forschungszentrum Juelich, Juelich, Germany*

Introduction

Detachment studies at AUG in L- and H-mode revealed that, when the inner divertor is strongly detached while the outer one remains attached, the ionization front close to the inboard separatrix has moved to the X-point and electron densities of the order of $10^{20}\,\mathrm{m}^{-3}$ are measured spectroscopically at the X-point. Simultaneously, radiative fluctuations appear in the high field side (HFS) divertor close to the X-point and a second high density region ($\sim 10^{20}\,\mathrm{m}^{-3}$) forms in the scrape-off layer (SOL) at the HFS [1]. In H-mode, this so called HFS high density (HFSHD) spans out to $\rho_{pol} \approx 1.15$ (or 10 times the power decay length λ_q) into the far SOL and extends well above the X-point, measured independently by spectroscopy and interferometry [2]. Furthermore, in the all-tungsten AUG, high performance discharges are usually conducted with medium to high gas fuelling rates where the HFSHD is always present. Seeding of impurities has been shown to improve the plasma confinement [3, 4], and also reduces the HFSHD and the corresponding neutral flux density $\Gamma_{n,\mathrm{HFS}}$ (typically by $50-70\,\%$).

Here, we will discuss the influence of the heating power, edge density, fuelling rate and plasma current on n_e and the spatial extent of the HFSHD and show that there is a correlation between the $n_{e,HFSHD}$ reduction and confinement improvement due to impurity seeding.

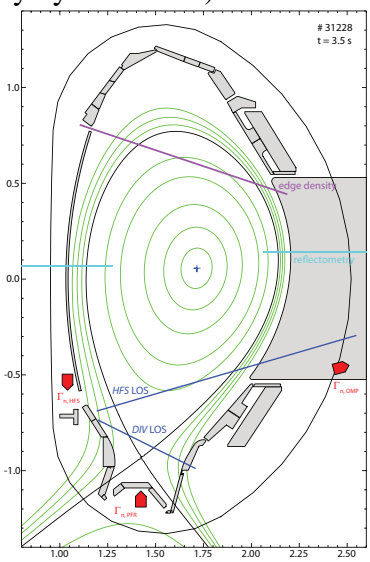

Figure 1: *DIV* & *HFS* LOS, neutral pressure gauges (red), reflectometry (cyan) and edge density interferometer (purple)

Discharge and diagnosic overview

The main diagnostics used to investigate the HFSHD are shown in figure 1. The local n_e in the inner divertor and HFS SOL is determined by Stark broadening analysis (SBD) of the spectroscopically measured Balmer D_ε line [6]. While the spectroscopic system covers the entire divertor region, we focus here only on two lines of sight (LOS), named *DIV* and *HFS* view. The two LOS intersect also the LFS SOL, but the D_ε emission in this region is more than one order of magnitude lower than the emission in the inner divertor and thus negligible. In addition, two reflectometers measure the n_e profiles at the LFS and HFS mid-plane [5]. Neutral fluxes are measured with AUG pressure gauges. The gauges used here are situated at the entrance to the inner divertor, at the outer mid-plane and below the divertor private flux region (PFR).

For this work, a set of 27 lower single null H-mode discharges with a magnetic field of $B_T = -2.5\,\mathrm{T}$ and a plasma current of 0.8 or 1.0 MA has been analyzed. The inner divertor plasma is always detached at the vertical target component (flat ion saturation current profile) whereas the outer divertor plasma remains attached. The total additional heating power P_{TOT} in this database

*See http://www.euro-fusionscipub.org/mst1

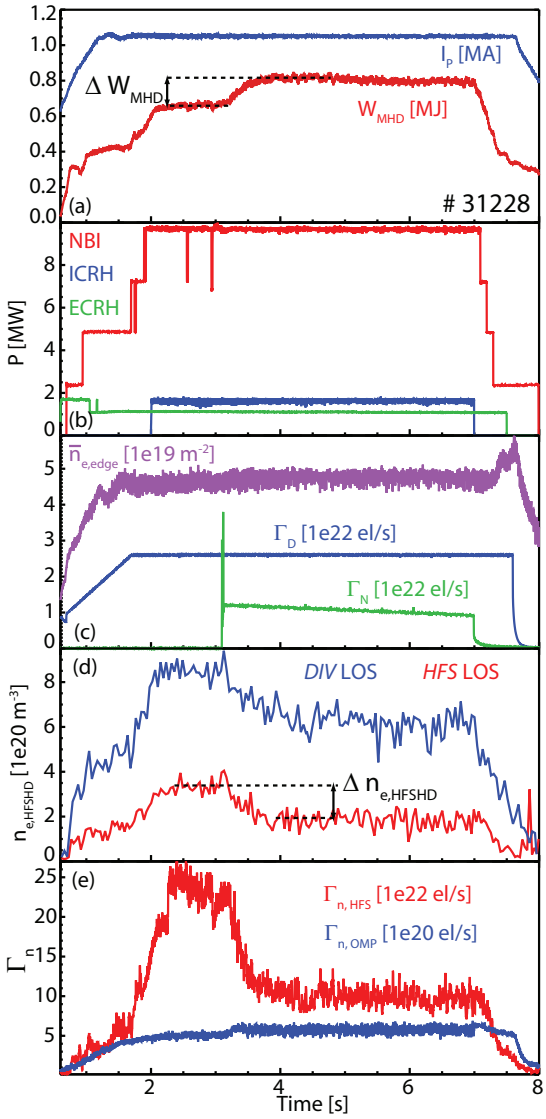

Figure 2: Time traces of a typical discharge of the database. See text for explanation

spans from $3-16\,\mathrm{MW}$, consisting mainly of neutral beam heating (NBI), electron cyclotron heating $P_{ECH} \leq 2\,\mathrm{MW}$ and, in some case, ion cyclotron heating $P_{ICH} \leq 4\,\mathrm{MW}$. The feed forward gas fuelling rate varies from $6\times10^{20}-3.4\times10^{22}\mathrm{el/s}$. Figure 2 shows time traces of a typical discharge from the database. During the current ramp up phase of the discharge, the plasma fuelling and the heating power are simultaneously increased. In the flat-top phase of the discharge, the fuelling is kept constant, resulting in an approximately constant main plasma density and divertor neutral pressure, and the heating power is increased further. Correlated with the increase of the heating power the HFSHD develops. During the highest heating phase, densities of $8.5\times10^{20}\,\mathrm{m}^{-3}$ and $3.4\times10^{20}\,\mathrm{m}^{-3}$ are measured with the *DIV* and *HFS* LOS (see Fig. 1), respectively, which is more than one order of magnitude larger than the separatrix density. The neutral fluxes in this region, $\Gamma_{n,HFS}$ increase up to $2.5\times10^{23}\,\mathrm{el/s}$, which is about 500 times the neutral fluxes at the outer mid-plane $\Gamma_{n,mp}$, see Figure 2e. Moreover, the n_e profiles at the HFS and LFS mid-plane are similar before the HFSHD formation with a separatrix density of $n_{e,sep}\approx3\times10^{19}\,\mathrm{m}^{-3}$. When the HFSHD is present, the LFS n_e profile is almost unchanged, but at the HFS a density of $n_e=6\times10^{19}\,\mathrm{m}^{-3}$ (which is the maximal measurable density of the reflectometry system) is measured at a normalized poloidal radius of $\rho_{pol}\approx1.09$. For details see [5]. Later in the discharge, nitrogen (sometimes also krypton in addition to nitrogen) is injected into the divertor private flux region while the heating power is kept constant. The impurity seeding leads to an increase of the plasma stored energy W_{MHD} from 600 to 800 kJ and also reduces n_e and $\Gamma_{n,HFS}$ in the HFSHD region.

High field side high density scaling

This section evaluates the dependence of the HFSHD on P_{TOT}, I_p (or q_{95} as B_T is constant), the plasma fuelling and the main plasma density. Figures 3a-d shows n_e measured with the *DIV* and *HFS* LOS versus P_{TOT} for $I_p=0.8\,\mathrm{MA}$ and $I_p=1.0\,\mathrm{MA}$, respectively. The color scale represents the applied deuterium fuelling. The increase of the HFSHD with P_{TOT} is clearly visible in both LOS and both currents. For the *DIV* LOS, i.e. at the entrance of the inner divertor, it is at a given P_{TOT} approximately independent of I_p (q_{95}), see Fig. 3a,b. In contrast, in the HFS SOL (*HFS* LOS), n_e is higher in $I_p=0.8\,\mathrm{MA}$ discharges at a given P_{TOT}. Thus, the spatial extent of the HFSHD from the entrance to the inner divertor towards the HFS mid-plane is larger with lower I_p (higher q_{95}). This is revealed in Fig. 3e, where $n_{e,HFSHD}(DIV)-n_{e,HFSHD}(HFS)$ is shown. Furthermore, the poloidal gradient (as well as the absolute value) of $n_{e,HFSHD}$ towards the HFS mid-plane increases with heating power, independent of I_p (q_{95}). In order to

disentangle the dependence of the fuelling and plasma density on the HFSHD, we first need to discuss the effect of Γ_D on $n_{e,edge}$. In 1.0 MA discharges, the plasma density does not change with fuelling levels $\Gamma_D \geq 0.5 \times 10^{22}$ el/s (Fig. 3f). Hence, the increase of the HFSHD at a given P_{TOT} (Fig. 3a, c) is due to the fuelling rate Γ_D and independent of $n_{e,edge}$. However, with $I_p = 0.8$ MA, there is a clear increase of $n_{e,edge}$ with increasing Γ_D until $\Gamma_D \approx 1.8 \times 10^{22}$ el/s, then $n_{e,edge}$ almost saturates. The increase of the HFSHD at a given $P_{TOT} \leq 7$ MW (Fig. 3b,d) is thus caused by the increase of $n_{e,edge}$. Above $P_{TOT} = 7$ MW, the increase of the HFSHD at a given P_{TOT} is smaller and mainly caused by the increased fuelling rate. To sum this up, as long as $n_{e,edge}$ can be increased with the fuelling rate Γ_D, there is a strong, indirect influence of Γ_D on the HFSHD via the $n_{e,edge}$ increase. Otherwise, the HFSHD still increases with Γ_D, but this is a smaller effect. Finally, there is a clear correlation between the HFSHD and the neutral fluxes in HFS SOL $\Gamma_{n,HFS}$, as shown in Figure 3g,h. The increase of the HFSHD with $\Gamma_{n,HFS}$ is independent of P_{TOT}, $n_{e,edge}$ and the fuelling rate Γ_D, but there is a different scaling for different I_p (q_{95}). Moreover, at a given $\Gamma_{n,HFS}$, the HFSHD extent is larger at lower I_p (higher q_{95}). It is important to note that there is no correlation between the HFSHD and the neutral fluxes in the PFR, i.e. the divertor neutral pressure (not shown).

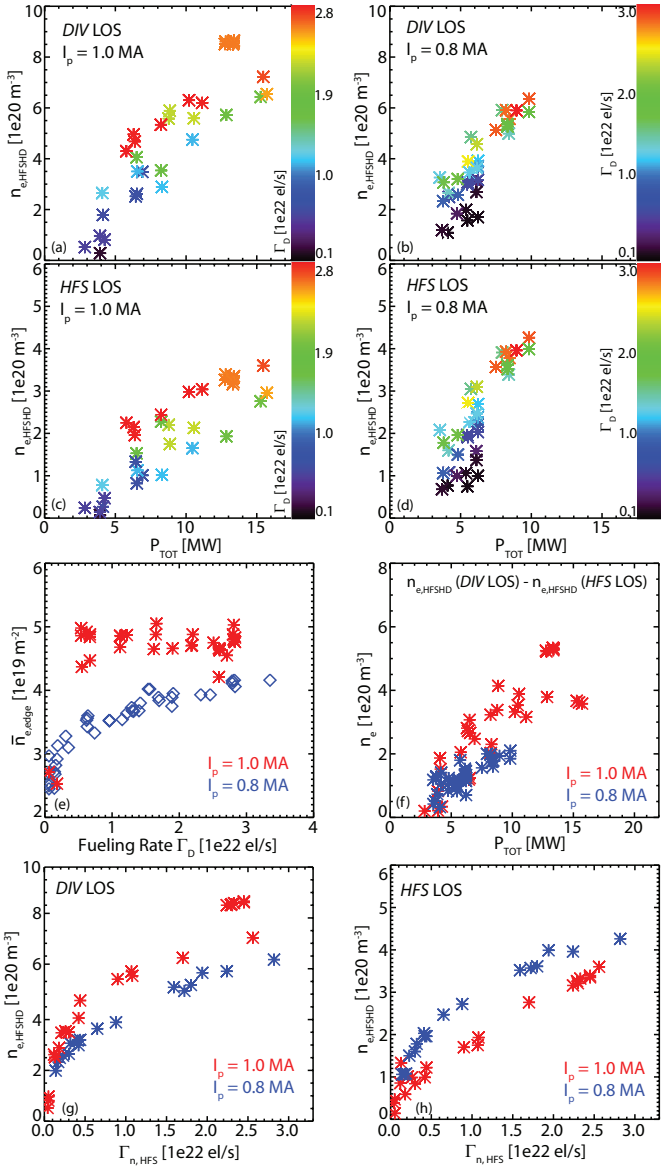

Figure 3: (a-d) HFSHD versus total heating power, (e) edge density versus fuelling rate, (f) difference of *DIV* & *HFS* LOS versus total heating power, (g-h) HFSHD versus neutral fluxes in the HFS SOL.

Correlation between the reduction of the HFSHD and confinement improvement due to impurity seeding

As already mentioned above, seeding of impurities leads to a reduction of the HFSHD and also to an increase of the stored energy W_{MHD}. Figures 4a,b reveal their correlation, where the HFSHD reduction $\Delta n_{e,HFSHD}$ is plotted against the confinement improvement ΔW_{MHD}, which are the differences of the two quantities before and during the impurity seeding (see Fig. 2). Independent of the impurity species, ΔW_{MHD} increases clearly with the absolute value of $\Delta n_{e,HFSHD}$ for both, the *DIV* and *HFS* LOS. Moreover, the more N_2 is injected, the stronger is $\Delta n_{e,HFSHD}$, which is in Fig. 4c, only shown for the *HFS* LOS, but the *DIV* LOS is similar. Note that the abscissa shows the injected impurity atoms per second. If on top of N_2 Kr is injected ($\Gamma_{Kr} \leq 3.5 \times 10^{19}$ atoms/s), the HFSHD is reduced even further, which reveals that Kr has the similar effect as N_2 on the HFSHD. Moreover, as about 2 orders of magnitude less Kr atoms are

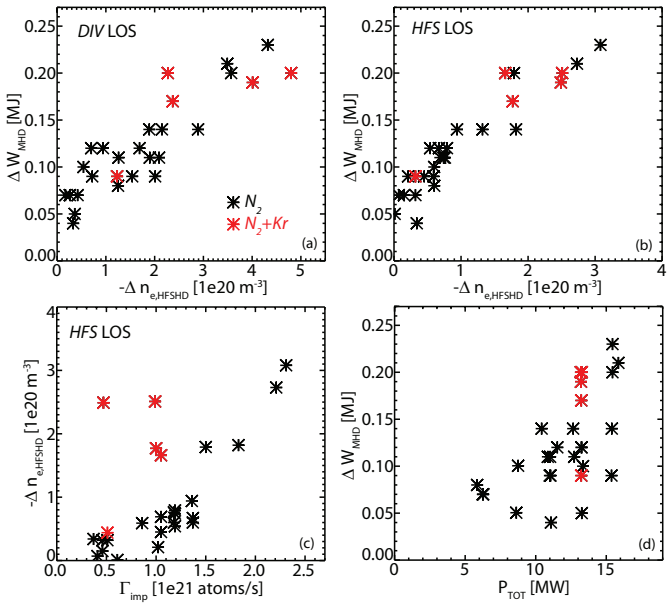

Figure 4: (a,b) Confinement improvement versus HFSHD reduction for the *DIV* & *HFS* LOS, (c) HFSHD reduction versus the impurity seeding rate in atoms per second for the *DIV* LOS, (d) Confinement improvement versus total heating power.

injected compared to N indicates that the amount of atoms (e.g. Z_{eff}) is not what matters for the $\Delta n_{e,HFSHD}$ and ΔW_{MHD} increase, but the amount of power which can be radiated per impurity atom (L_Z). Finally, at higher heating power a stronger confinement improvement can be achieved (Fig. 4f), depending on the impurity injection rate. This is consistent with the observations that the HFSHD is larger at higher P_{TOT}. Therefore, a higher $\Delta n_{e,HFSHD}$ and hence ΔW_{MHD} can be reached, given that enough impurities are injected. It must be noted that the outer divertor always remains attached in this database and, thus, at higher P_{TOT} it is also possible to inject more impurities.

Conclusions

All together, this indicates that the HFSHD and the correlated neutral fluxes $\Gamma_{n,HFS}$ are governed by the local recycling in the inner divertor, which is mainly determined by $n_{e,edge}$ and the power reaching the HFS SOL. The recycling fluxes under these conditions are about $1-2$ orders of magnitude larger than the gas fuelling rate, which has only a weaker effect on the HFSHD. Moreover, the spatial extent of the HFSHD is smaller at higher I_p (q_{95}).

Finally, there is a clear correlation between the reduction of the HFSHD $\Delta n_{e,HFSHD}$ and the confinement improvement ΔW_{MHD} due to impurity seeding. The higher $\Delta n_{e,HFSHD}$, the stronger ΔW_{MHD}, irrespective of the impurity species. Consequently, at higher P_{TOT} and hence higher $n_{e,HFSHD}$, a higher ΔW_{MHD} can be achieved, provided that there is enough impurity injection, which radiates power in the SOL, to reach a high $\Delta n_{e,HFSHD}$. This is all consistent with the fact that in the old AUG and JET C-machines the confinement was generally better due to different operational boundary conditions such as the fuelling [7]. Similar to N, C radiates mainly in the SOL and is always present in the SOL as it is produced even at low temperatures via chemical sputtering. Hence, the HFSHD, which was also observed in AUG-C [8], could be intrinsically reduced in C-machines, leading to a better confinement. The correlation between $\Delta n_{e,HFSHD}$ and ΔW_{MHD} due to impurity seeding can only be quantitatively investigated, however, with extensive 2D simulation codes such as SOLPS, where the HFSHD has not been successfully reproduced yet.

Acknowledgment

This work has been carried out within the framework of the EUROfusion Consortium and has received funding from the Euratom research and training programme 2014-2018 under grant agreement No 633053. The views and opinions expressed herein do not necessarily reflect those of the European Commission.

References

[1] S. Potzel, et al., NF **54** 0130011 (2014)
[2] S. Potzel, et al., JNM, (2015)
[3] J. Schweinzer, et al., NF **51** 113003 (2011)
[4] M. Dunne, et al., *This conference*
[5] L. Guimarais, et al., *This conference*
[6] S. Potzel, et al., PPCF, **56**, 025010 (2014)
[7] M. Beurskens, et al., PPCF, **55**, 124043 (2013)
[8] K. McCormick, et al., JNM, **390**, S465 (2009)